Electronic Supplementary Material (ESI) for RSC Advances.

Supplementary Information

Diorganotin(IV) 4,6-dimethyl-2-pyrimidyl selenolates: Synthesis, structures and their utility as molecular precursors for the preparation of $SnSe_2$ nano-sheets and thin films

Adish Tyagi, G. Kedarnath, Amey Wadawale, Alpa Y. Shah, Vimal K. Jain and B. Vishwanadh

Figure Captions:

Fig. S24 a) Simulated XRD pattern of hexagonal $SnSe_2$ (JCPDS-40-1465). XRD profiles of $SnSe_2$ nanosheets obtained by b) thermolysis of $[Et_2Sn\{SeC_4H(Me\text{-}4,6)_2N_2\}_2]$ (**2**), c) $[^nBu_2Sn\{SeC_4H(Me\text{-}4,6)_2N_2\}_2]$ (**3**) and d) $[^tBu_2Sn\{SeC_4H(Me\text{-}4,6)_2N_2\}_2]$ (**4**) in OLA at 210 ^oC for 5 minutes ('*' indicates the impurity peak of Se).

Fig. S25 a) Simulated XRD pattern of hexagonal $SnSe_2$ (JCPDS-23-0602). XRD profiles of $SnSe_2$ nanosheets obtained by b) thermolysis of $[Et_2Sn\{SeC_4H(Me\text{-}4,6)_2N_2\}_2]$ (**2**), c) $[^nBu_2Sn\{SeC_4H(Me\text{-}4,6)_2N_2\}_2]$ (**3**) and d) $[^tBu_2Sn\{SeC_4H(Me\text{-}4,6)_2N_2\}_2]$ (**4**) in OLA at 210 ^oC for 10 minutes.

Fig. S26. SEM images of $SnSe_2$ nanosheets obtained by a) thermolysis of $[Et_2Sn\{SeC_4H(Me\text{-}4,6)_2N_2\}_2]$ (**2**), b) $[^tBu_2Sn\{SeC_4H(Me\text{-}4,6)_2N_2\}_2]$ (**4**) in OLA at 210 ºC for 10 minutes (Inset show magnified images of the same).

Fig. S27 XRD profile of $SnSe_2$ thin film obtained by AACVD of $[^tBu_2Sn\{SeC_4H(Me\text{-}4,6)_2N_2\}_2]$ (**4**) on silicon substrate at 375 ^oC for 1 h overlaid on simulated XRD pattern of hexagonal $SnSe_2$ (JCPDS-40-1465).

Fig. S28 Plots of $[F(R)h\nu]^2$ vs energy generated by Kubelka-Munk transformation of solid-state diffuse reflectance data of $SnSe_2$ nano-sheets obtained by thermolysis of $[Et_2Sn\{SeC_4H(Me\text{-}4,6)_2N_2\}_2]$ (**2**) in OLA at 210 ^oC for a) 2, b) 5 and c) 10 minutes, respectively for determining direct band gap energies.

Fig. S29 Plots of $[F(R)h\nu]^{1/2}$ vs energy generated by Kubelka-Munk transformation of solid-state diffuse reflectance data of $SnSe_2$ nano-sheets obtained by thermolysis of $[Et_2Sn\{SeC_4H(Me\text{-}4,6)_2N_2\}_2]$ (**2**) in OLA at 210 ^oC for a) 2, b) 5 and c) 10 minutes, respectively for determining indirect band gap energies.

Fig. S30 Plots of $[F(R)h\nu]^{1/2}$ vs energy generated by Kubelka-Munk transformation of solid-state diffuse reflectance data of $SnSe_2$ nano-sheets obtained by thermolysis of $[^tBu_2Sn\{SeC_4H(Me\text{-}4,6)_2N_2\}_2]$ (**4**) in OLA at 210 ^oC for a) 2, b) 5 and c) 10 minutes, respectively for determining indirect band gap energies.

Fig. 31 Plots of $[F(R)h\nu]^{1/2}$ vs energy generated by Kubelka-Munk transformation of solid-state diffuse reflectance data of a) as-deposited $SnSe_2$ thin films obtained by AACVD of $[^tBu_2Sn\{SeC_4H(Me\text{-}4,6)_2N_2\}_2]$ (**4**) on silicon substrate at 375 ^oC for 1 h and b) annealed thin films to determine indirect band gap energies.

Table S1 Crystallographic and structural determination data for $[^nBu_2Sn\{SeC_4H(Me\text{-}4,6)_2N_2\}_2]$ (**3**).

Table S2 Selected bond lengths (Å) and angles (^{o}) for $[^nBu_2Sn\{SeC_4H(Me\text{-}4,6)_2N_2\}_2]$ (**3**).

Table S3 XRD data for tin selenide nanosheets.

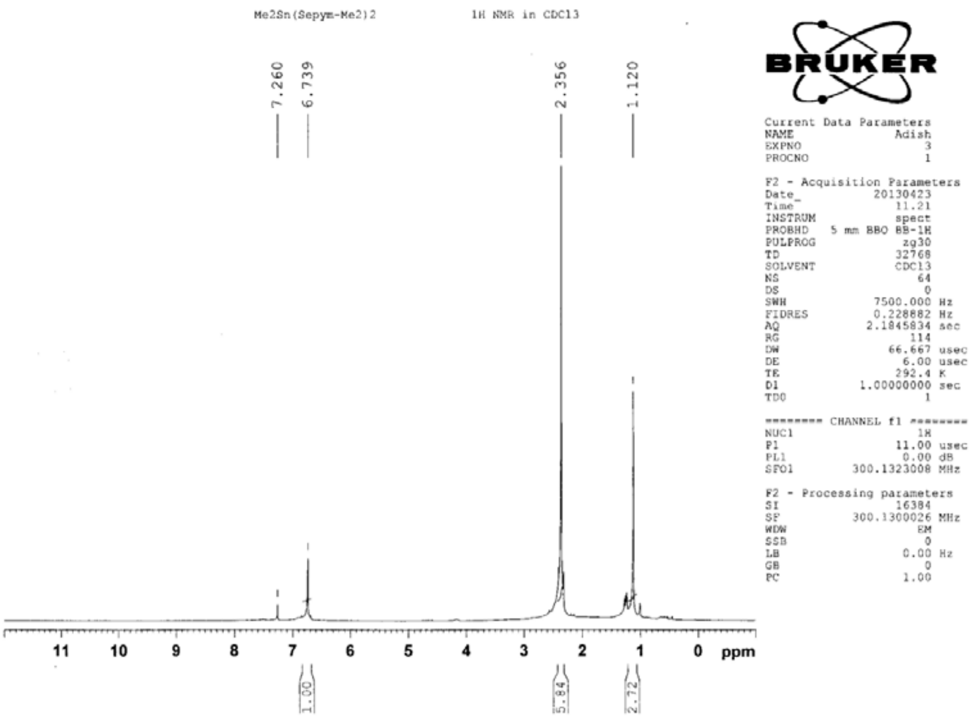

Fig. S1 ^{1}H NMR spectrum of [$Me_2Sn\{SeC_4H(Me\text{-}4,6)_2N_2\}_2$] (**1**) acquired in CDCl$_3$.

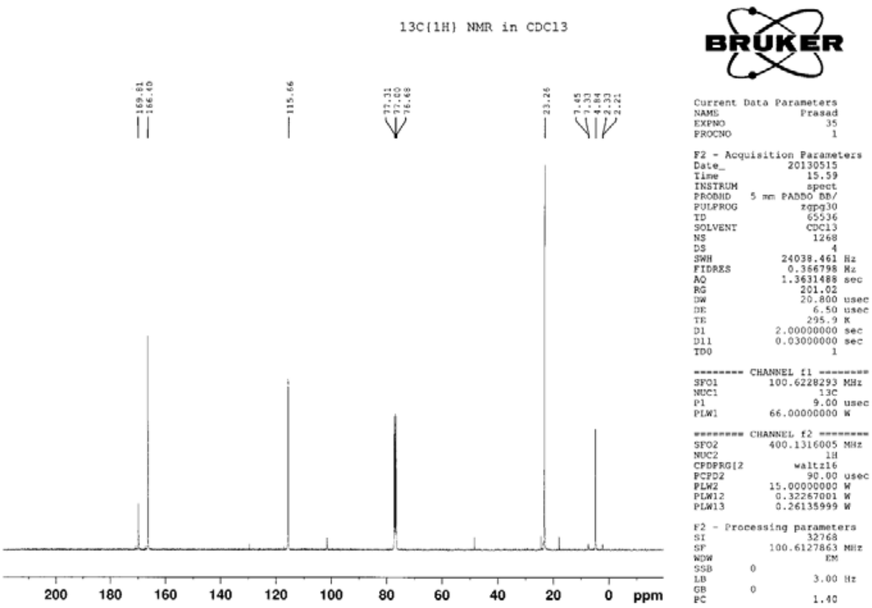

Fig. S2 $^{13}C\{^{1}H\}$ NMR spectrum of (**1**) acquired in CDCl$_3$.

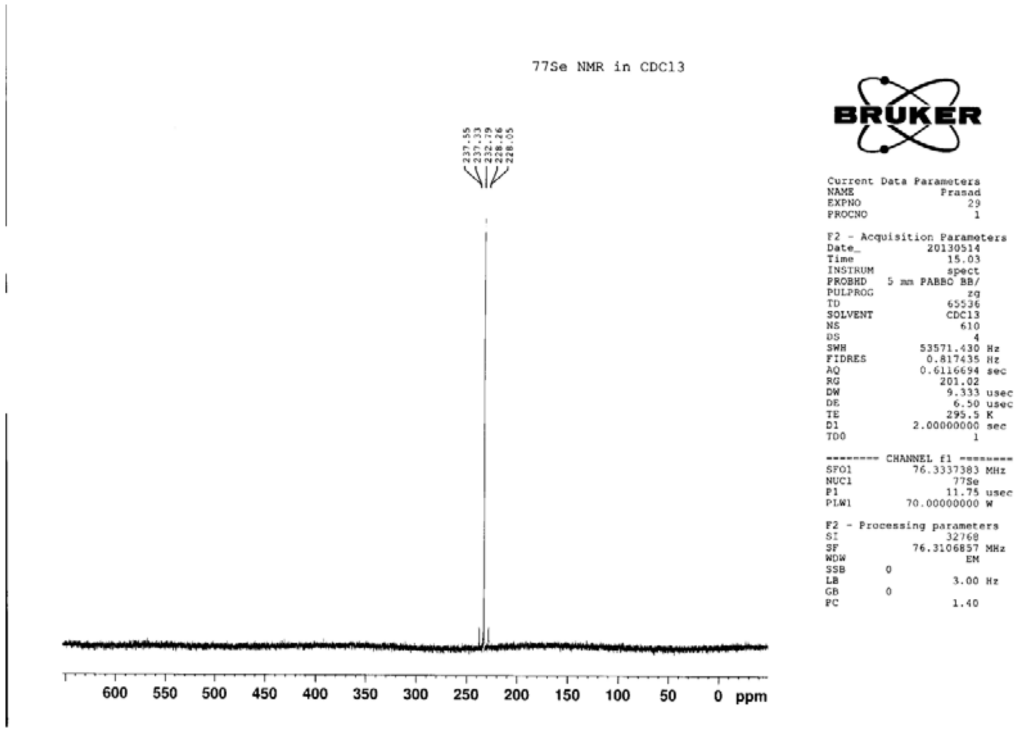

Fig. S3 ^{77}Se{^{1}H} NMR spectrum of [$Me_2Sn\{SeC_4H(Me\text{-}4,6)_2N_2\}_2$] (**1**) acquired in $CDCl_3$.

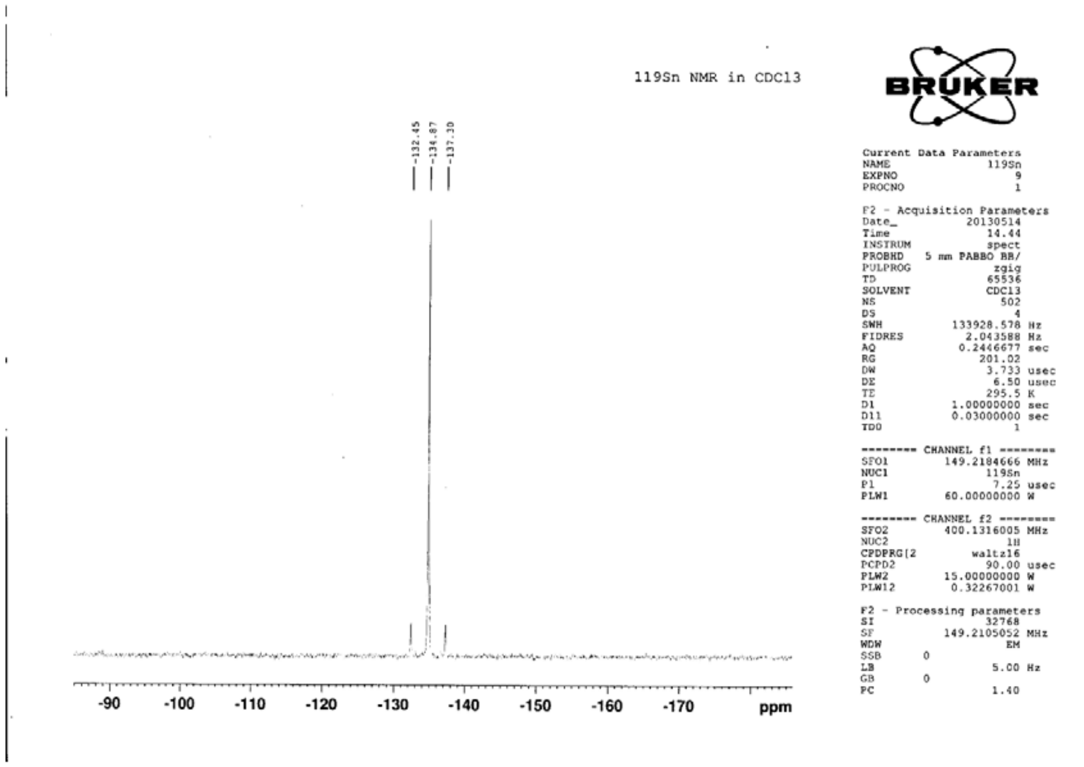

Fig. S4 ^{119}Sn{^{1}H} NMR spectrum of [$Me_2Sn\{SeC_4H(Me\text{-}4,6)_2N_2\}_2$] (**1**) acquired in $CDCl_3$.

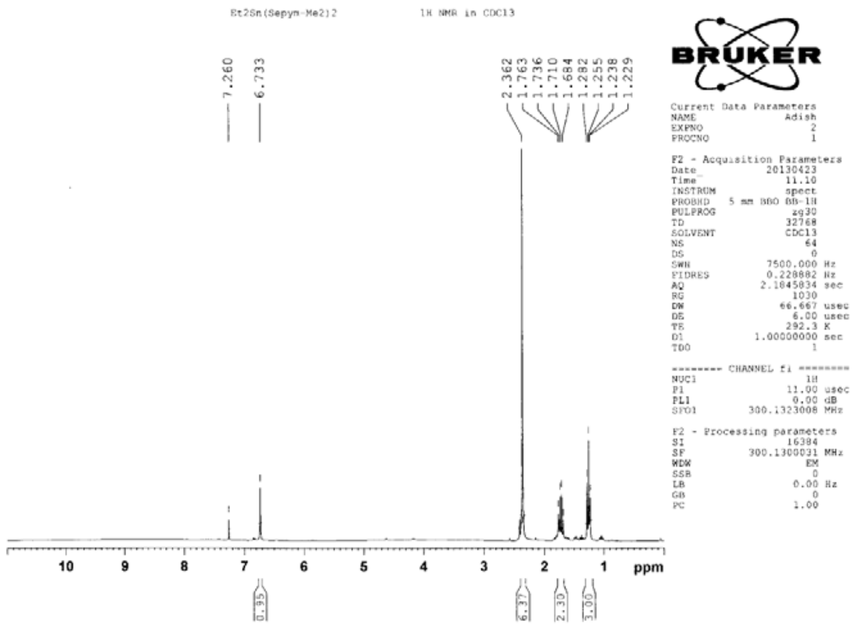

Fig. S5 [1]H NMR spectrum of $[Et_2Sn\{SeC_4H(Me\text{-}4,6)_2N_2\}_2]$ (**2**) acquired in $CDCl_3$.

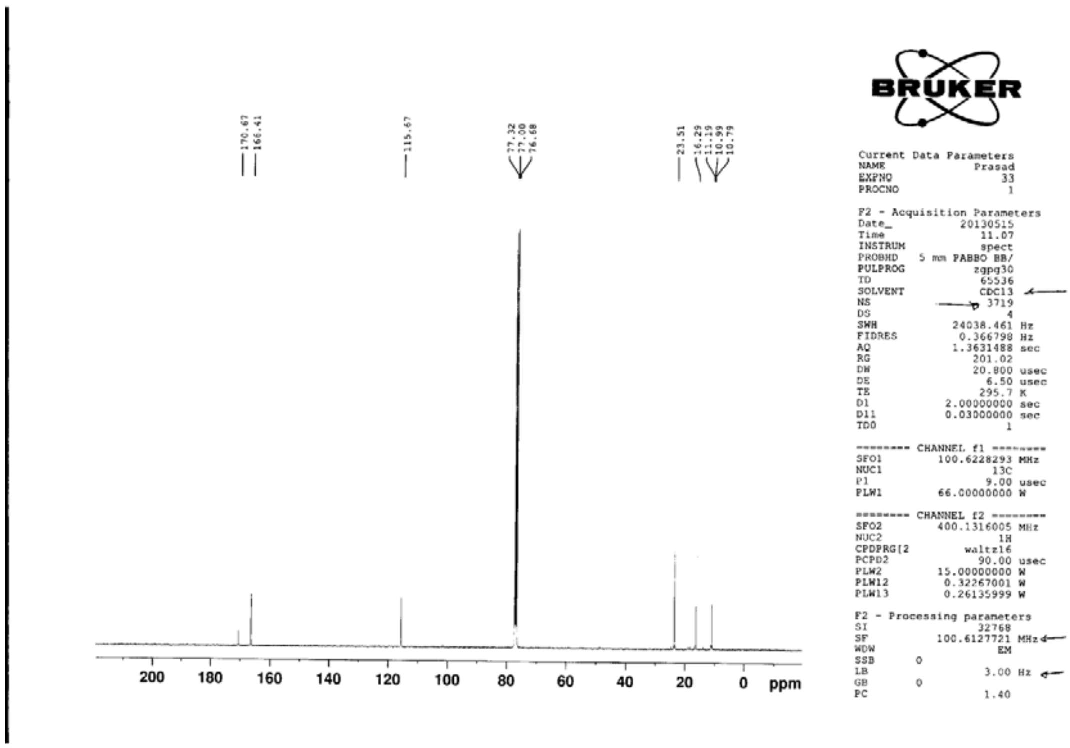

Fig. S6 [13]C{[1]H} NMR spectrum of $[Et_2Sn\{SeC_4H(Me\text{-}4,6)_2N_2\}_2]$ (**2**) acquired in $CDCl_3$.

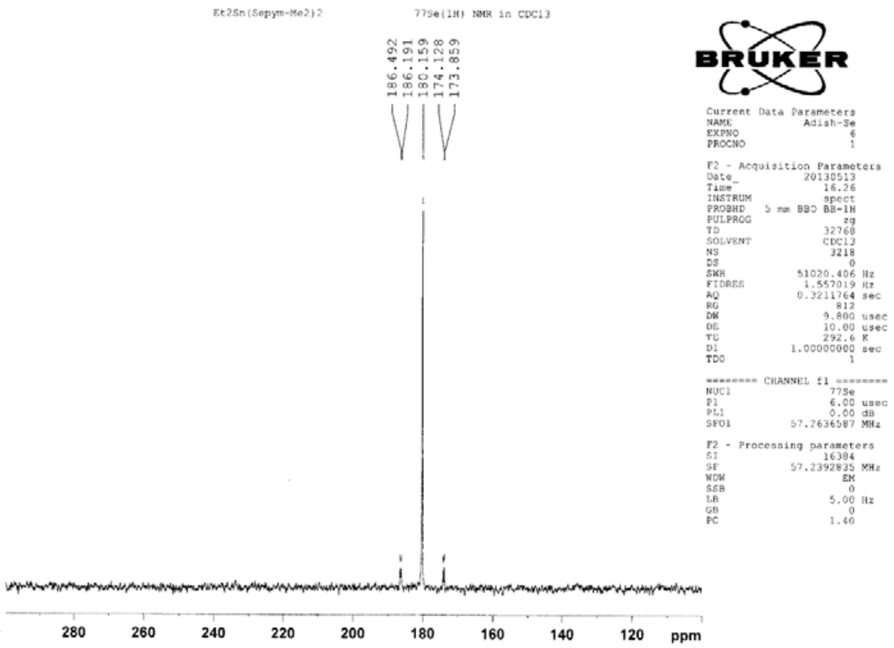

Fig. S7 ^{77}Se{^{1}H} NMR spectrum of [Et $_{2}$Sn{SeC$_{4}$H(Me-4,6)$_{2}$N$_{2}$}$_{2}$] (**2**) acquired in CDCl$_{3}$.

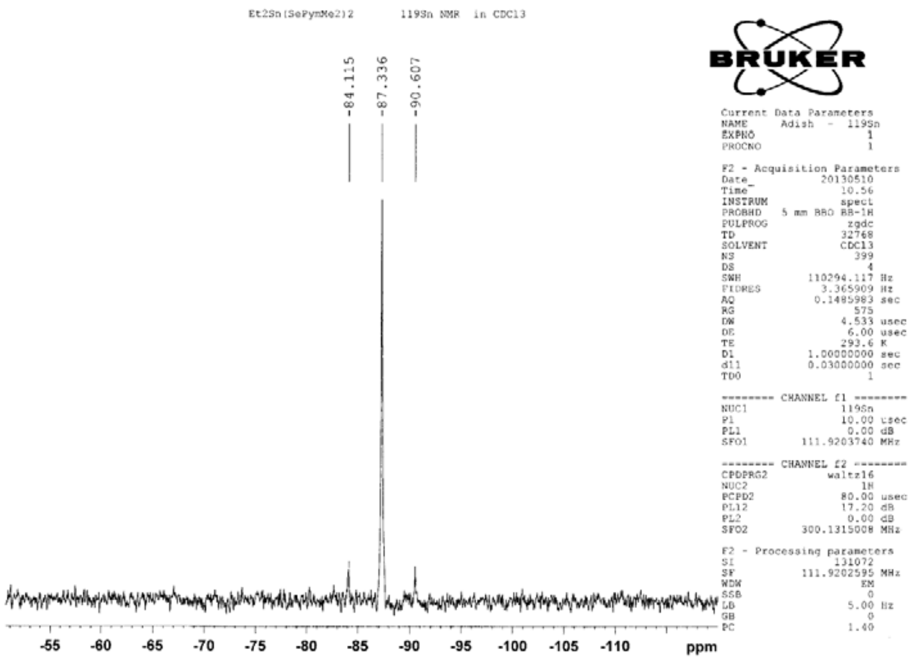

Fig. S8 ^{119}Sn{^{1}H} NMR spectrum of [Et $_{2}$Sn{SeC$_{4}$H(Me-4,6)$_{2}$N$_{2}$}$_{2}$] (**2**) acquired in CDCl$_{3}$.

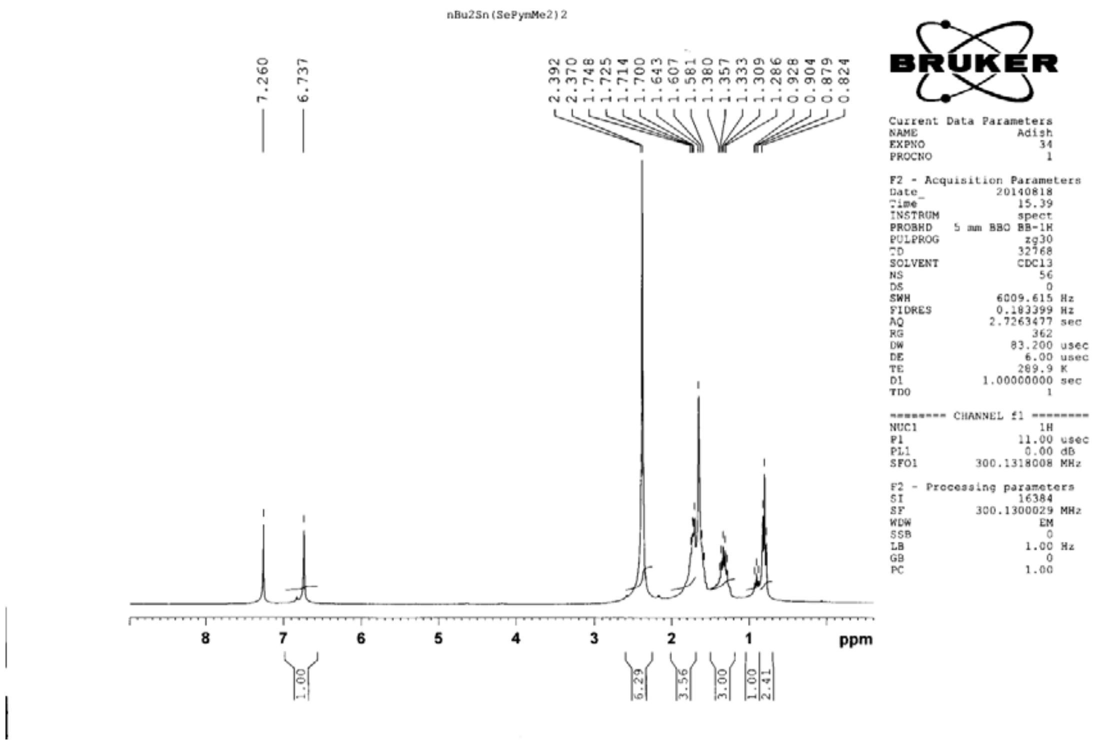

Fig. S9 ^{1}H NMR spectrum of [$^{n}Bu_2Sn\{SeC_4H(Me\text{-}4,6)_2N_2\}_2$] (**3**) acquired in CDCl$_3$.

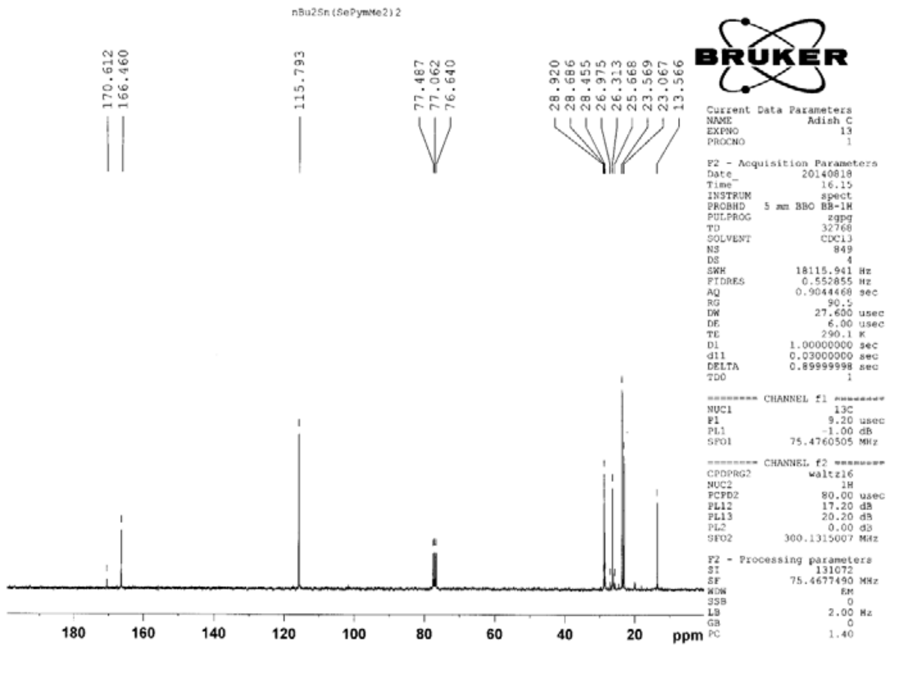

Fig. S10 $^{13}C\{^{1}H\}$ NMR spectrum of [$^{n}Bu_2Sn\{SeC_4H(Me\text{-}4,6)_2N_2\}_2$] (**3**) acquired in CDCl$_3$.

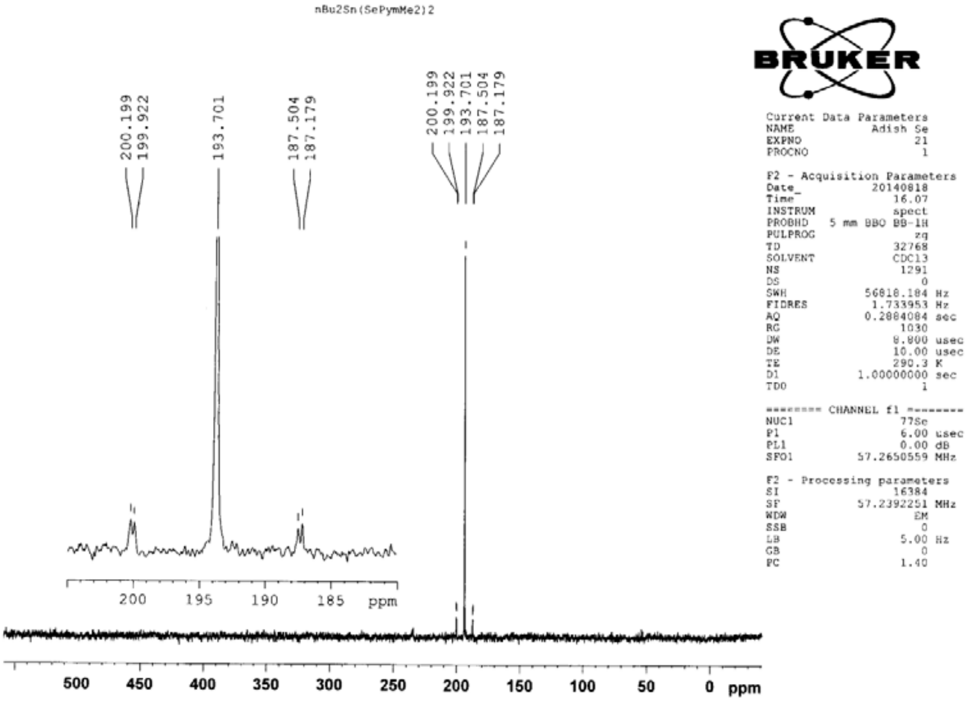

Fig. S11 $^{77}Se\{^1H\}$ NMR spectrum of $[^nBu_2Sn\{SeC_4H(Me\text{-}4,6)_2N_2\}_2]$ (**3**) acquired in CDCl$_3$.

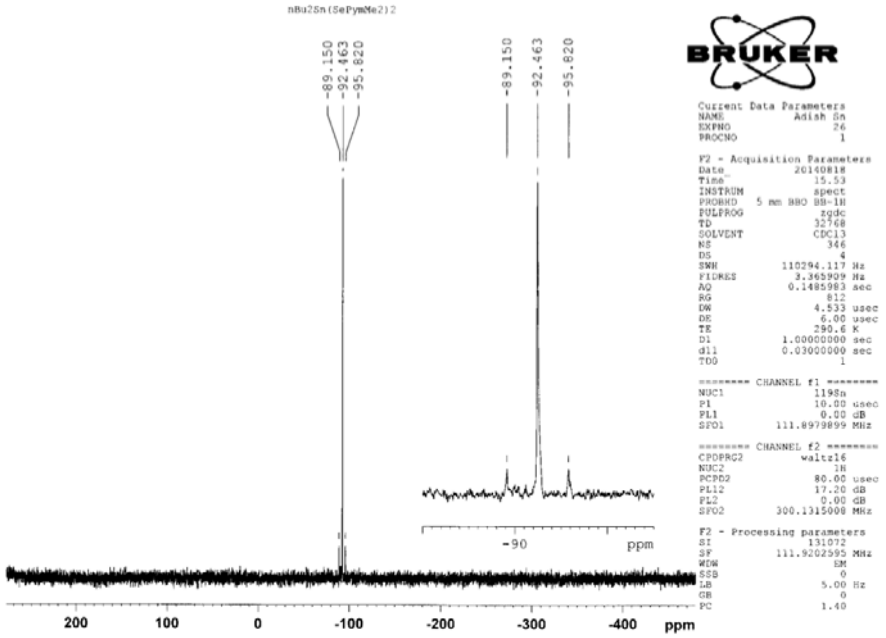

Fig. S12 $^{119}Sn\{^1H\}$ NMR spectrum of $[^nBu_2Sn\{SeC_4H(Me\text{-}4,6)_2N_2\}_2]$ (**3**) acquired in CDCl$_3$.

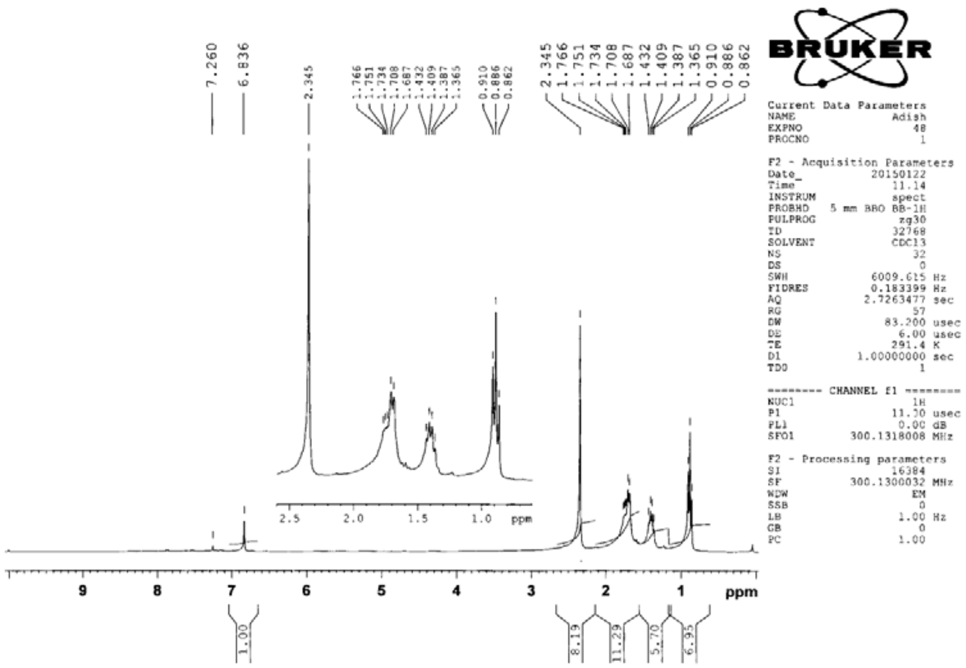

Fig. S13 [1]H NMR spectrum of [$^{n}Bu_2Sn\{SeC_4H(Me\text{-}4,6)_2N_2\}Cl$] (**6**) acquired in CDCl$_3$.

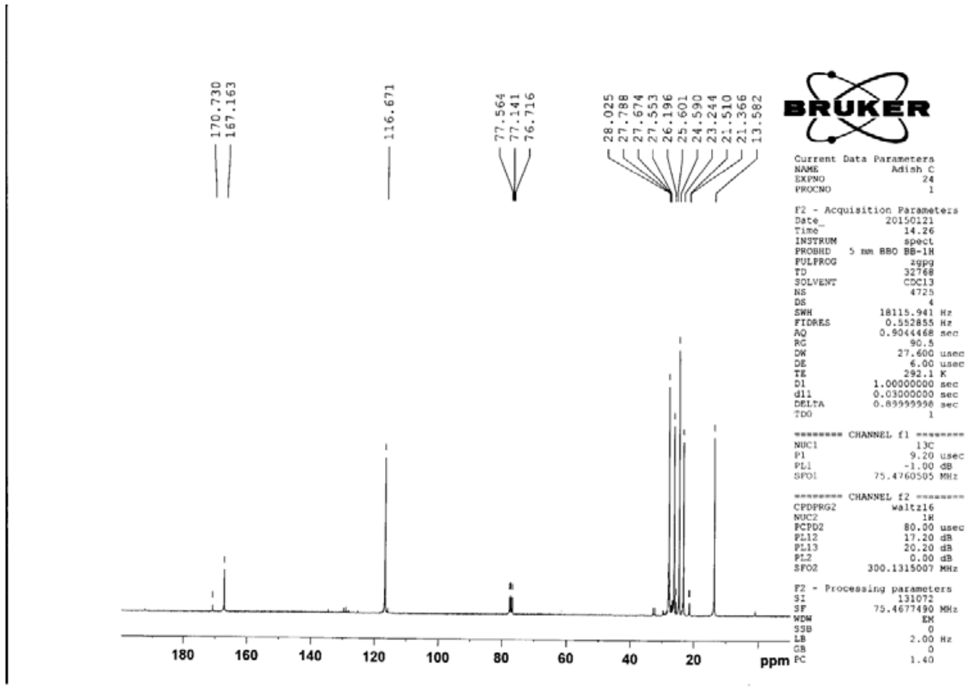

Fig. S14 [13]C{[1]H} NMR spectrum of [$^{n}Bu_2Sn\{SeC_4H(Me\text{-}4,6)_2N_2\}Cl$] (**6**) in CDCl$_3$

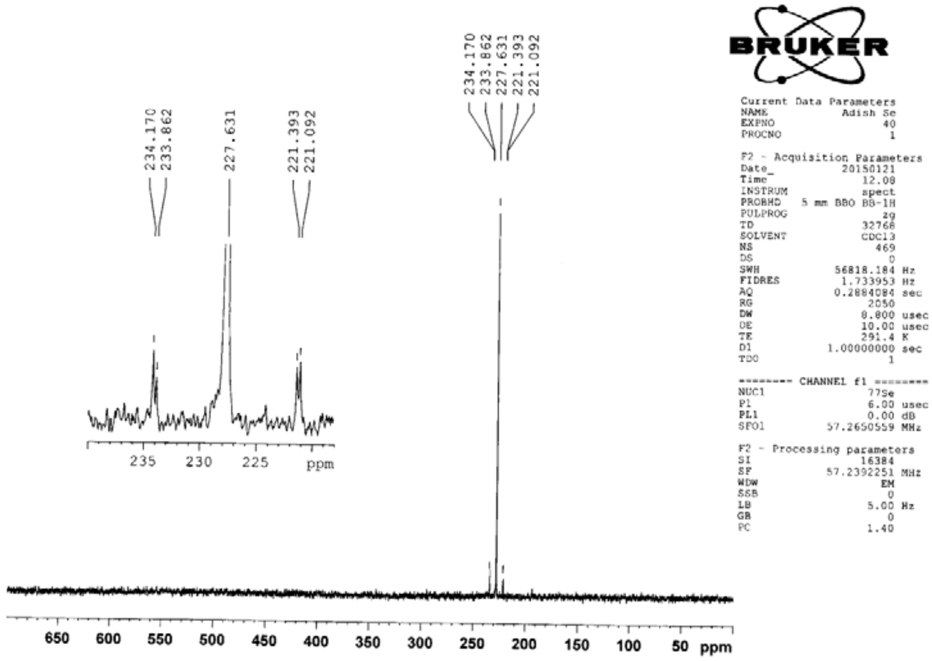

Fig. S15 $^{77}Se\{^1H\}$ NMR spectrum of $[^nBu_2Sn\{SeC_4H(Me\text{-}4,6)_2N_2\}Cl]$ (**6**) acquired in $CDCl_3$.

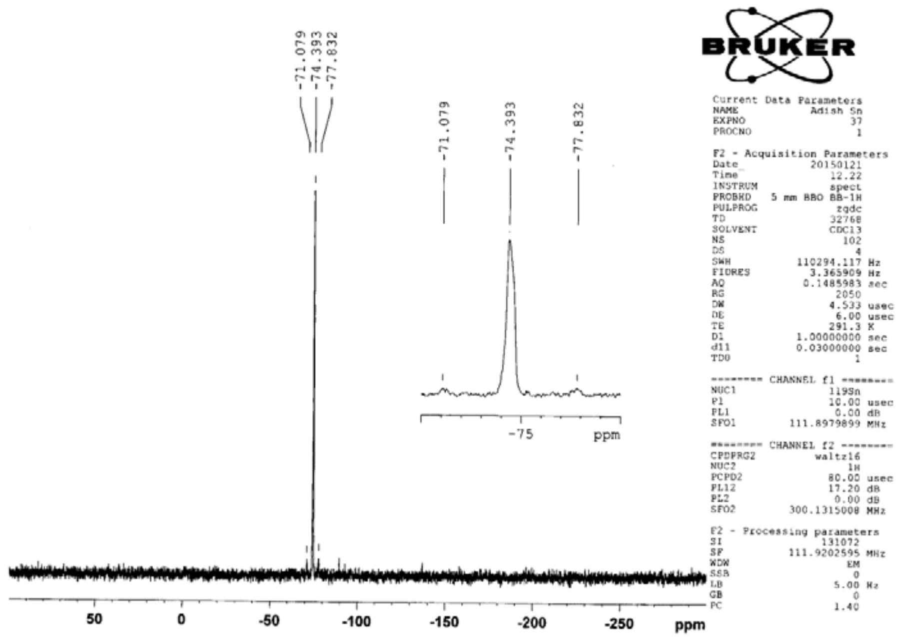

Fig. S16 $^{119}Sn\{^1H\}$ NMR spectrum of $[^nBu_2Sn\{SeC_4H(Me\text{-}4,6)_2N_2\}Cl]$ (**6**) acquired in $CDCl_3$.

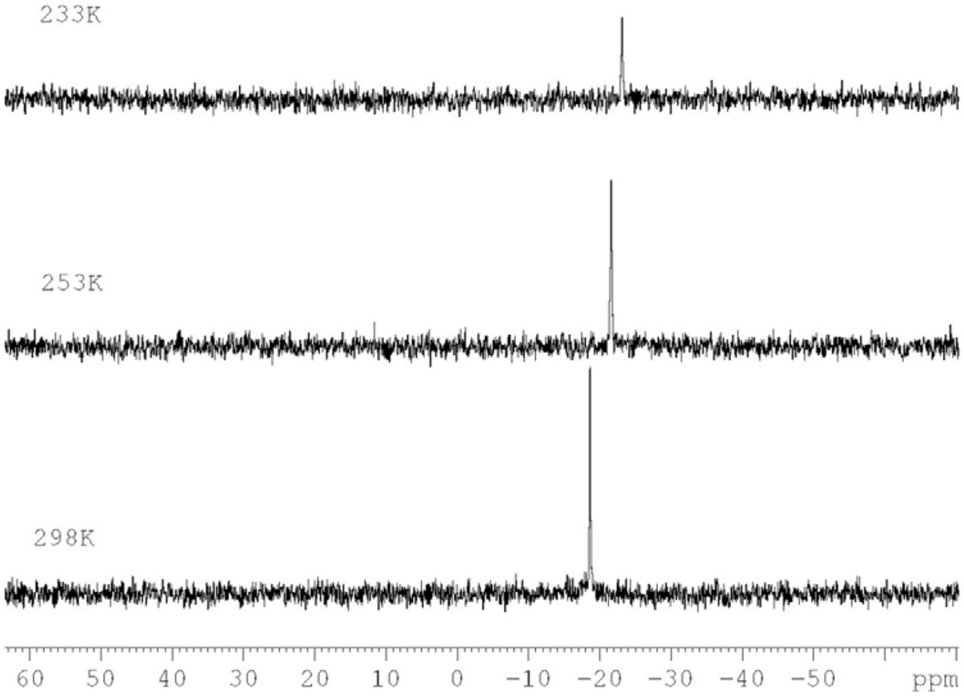

Fig. S17 Variable temperature $^{119}Sn\{^{1}H\}$ NMR spectrum of [$^{n}Bu_2Sn\{SeC_4H(Me\text{-}4,6)_2N_2\}Cl$] (**6**) acquired in $CDCl_3$.

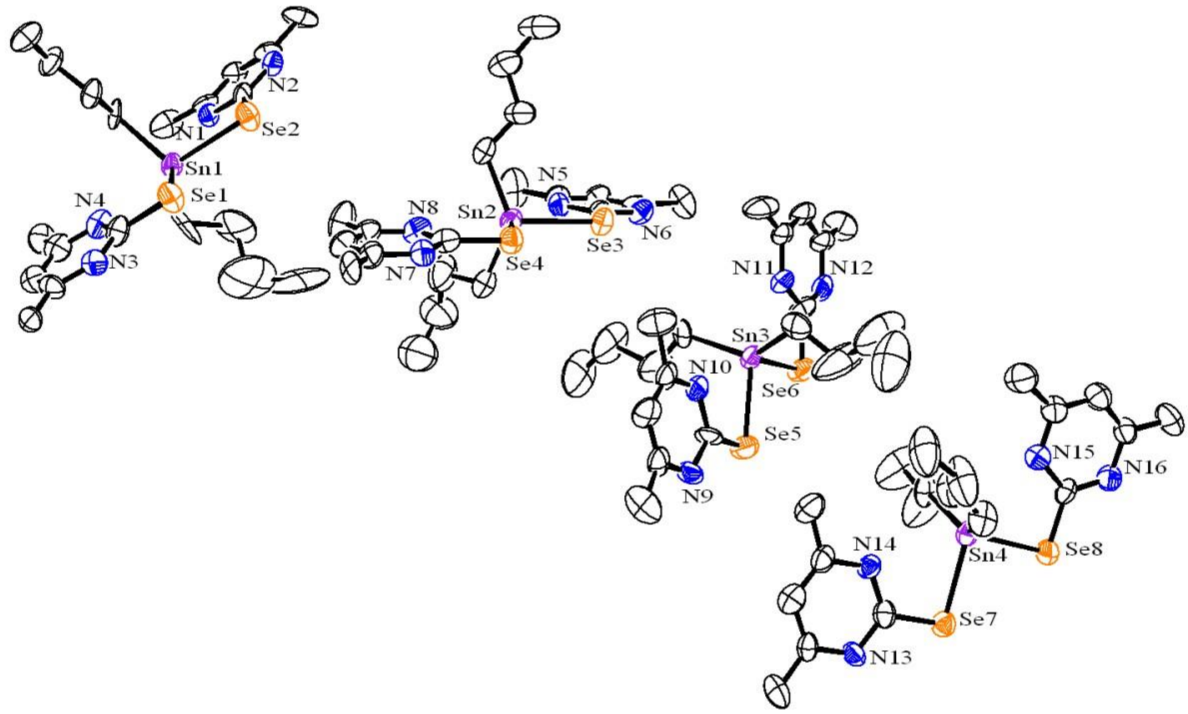

Fig. S18 ORTEP Diagram of [$^{n}Bu_2Sn\{SeC_4H(Me\text{-}4,6)_2N_2\}_2$] at 10% probability

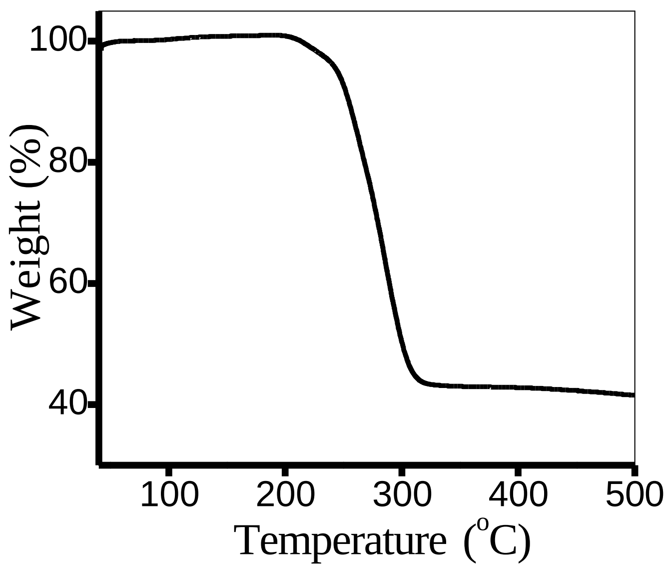

Fig. S19 TG curve of [$Me_2Sn\{SeC_4H(Me\text{-}4,6)_2N_2\}_2$] (**1**).

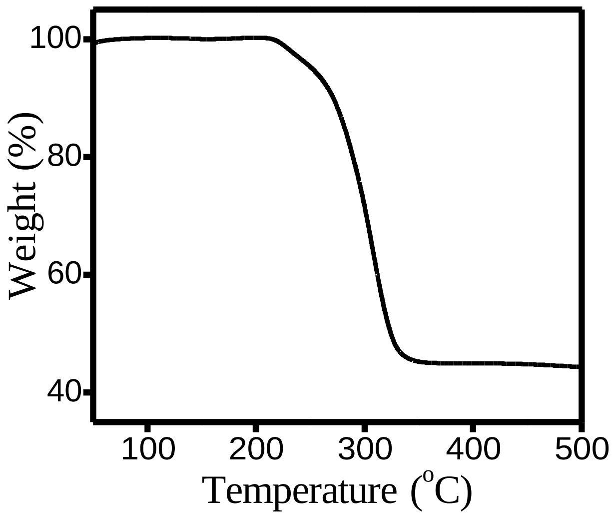

Fig. S20 TG curve of $[Et_2Sn\{SeC_4H(Me\text{-}4,6)_2N_2\}_2]$ (**2**).

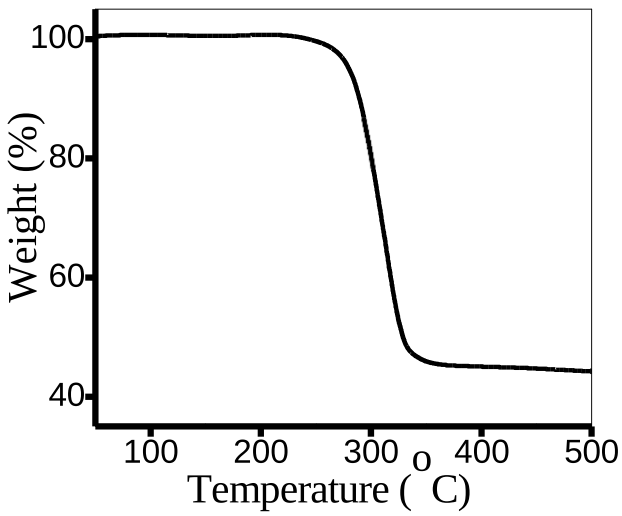

Fig. S21 TG curve of $[^nBu_2Sn\{SeC_4H(Me\text{-}4,6)_2N_2\}_2]$ (**3**).

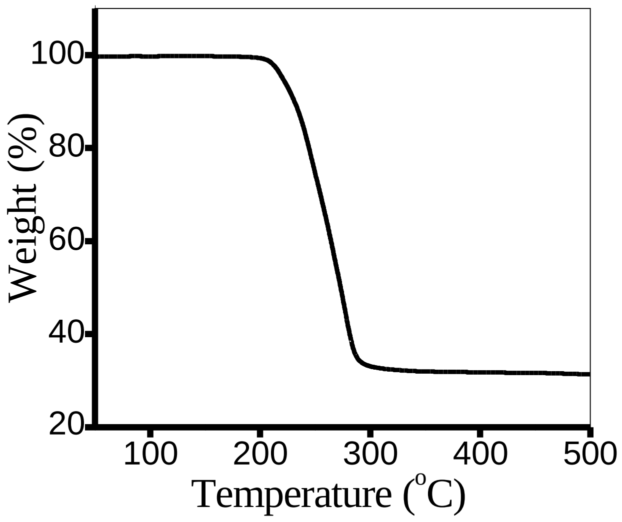

Fig. S22 TG curve of [$^{t}Bu_2Sn\{SeC_4H(Me\text{-}4,6)_2N_2\}_2$] (**4**).

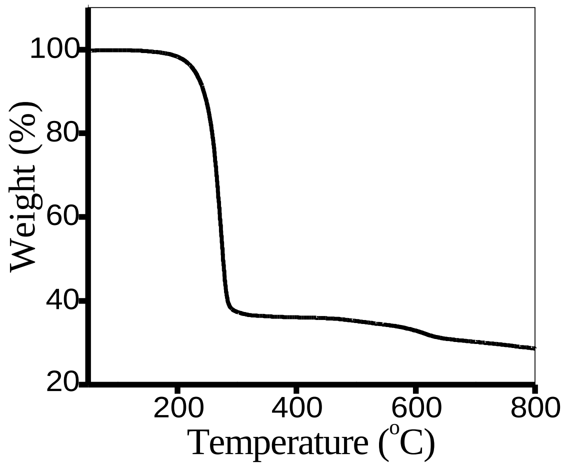

Fig. S23 TG curve of [$^{t}Bu_2Sn\{SeC_4H(Me\text{-}4,6)_2N_2\}Cl$] (**7**).

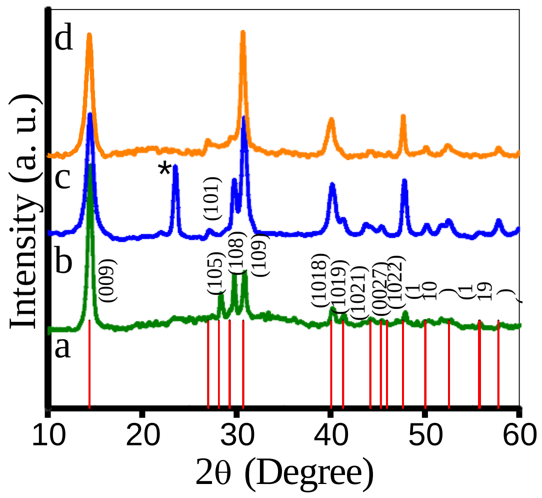

Fig. S24 a) Simulated XRD pattern of hexagonal $SnSe_2$ (JCPDS-40-1465). XRD profiles of $SnSe_2$ nanosheets obtained by b) thermolysis of $[Et_2Sn\{SeC_4H(Me\text{-}4,6)_2N_2\}_2]$ (**2**), c) $[^nBu_2Sn\{SeC_4H(Me\text{-}4,6)_2N_2\}_2]$ (**3**) and d) $[^tBu_2Sn\{SeC_4H(Me\text{-}4,6)_2N_2\}_2]$ (**4**) in OLA at 210 °C for 5 minutes ('*' indicates the impurity peak of Se).

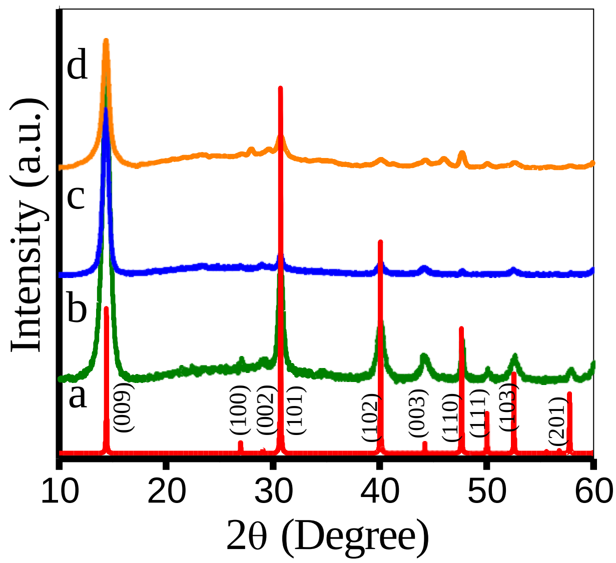

Fig. S25 a) Simulated XRD pattern of hexagonal $SnSe_2$ (JCPDS-23-0602). XRD profiles of $SnSe_2$ nanosheets obtained by b) thermolysis of $[Et_2Sn\{SeC_4H(Me\text{-}4,6)_2N_2\}_2]$ (**2**), c) $[^nBu_2Sn\{SeC_4H(Me\text{-}4,6)_2N_2\}_2]$ (**3**) and d) $[^tBu_2Sn\{SeC_4H(Me\text{-}4,6)_2N_2\}_2]$ (**4**) in OLA at 210 °C for 10 minutes.

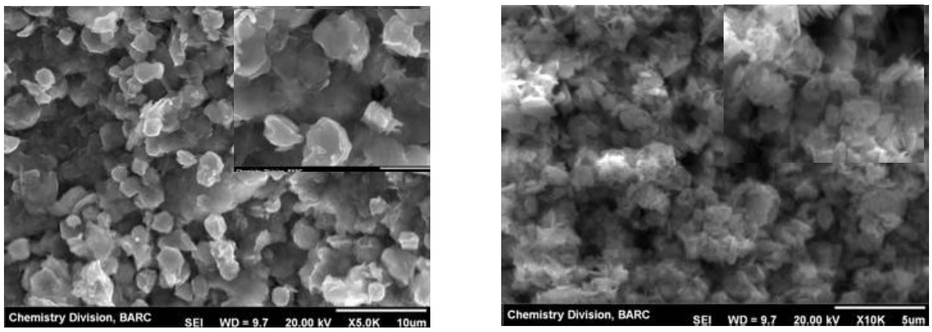

Fig. S26. SEM images of $SnSe_2$ nanosheets obtained by a) thermolysis of [$Et_2Sn\{SeC_4H(Me\text{-}4,6)_2N_2\}_2$] (**2**), b) [$^tBu_2Sn\{SeC_4H(Me\text{-}4,6)_2N_2\}_2$] (**4**) in OLA at 210 ºC for 10 minutes (Inset show magnified images of the same).

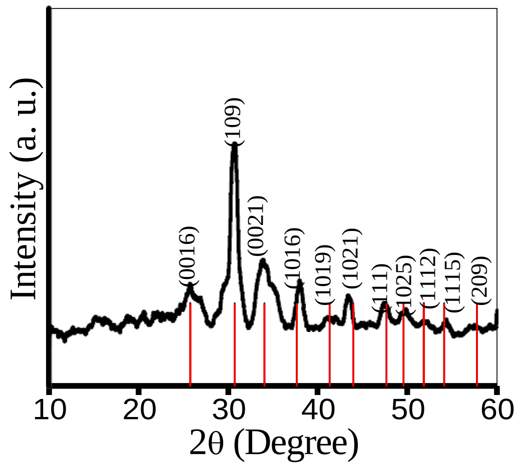

Fig. S27 XRD profile of $SnSe_2$ thin film obtained by AACVD of [$^tBu_2Sn\{SeC_4H(Me\text{-}4,6)_2N_2\}_2$] (**4**) on silicon substrate at 375 ^oC for 1 h overlaid on simulated XRD pattern of hexagonal $SnSe_2$ (JCPDS-40-1465).

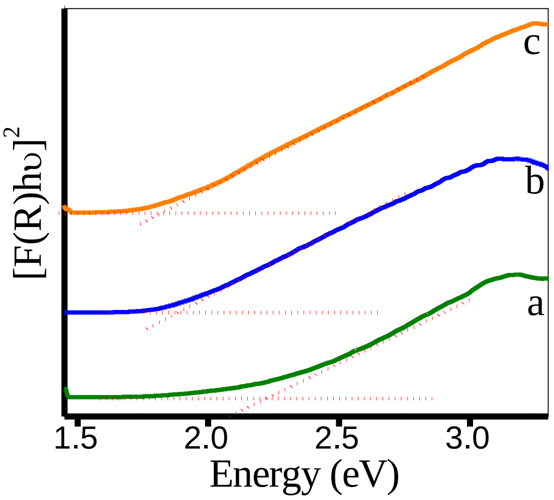

Fig. S28 Plots of $[F(R)h\nu]^2$ vs energy generated by Kubelka-Munk transformation of solid-state diffuse reflectance data of $SnSe_2$ nano-sheets obtained by thermolysis of $[Et_2Sn\{SeC_4H(Me\text{-}4,6)_2N_2\}_2]$ (**2**) in OLA at 210 °C for a) 2, b) 5 and c) 10 minutes, respectively for determining direct band gap energies.

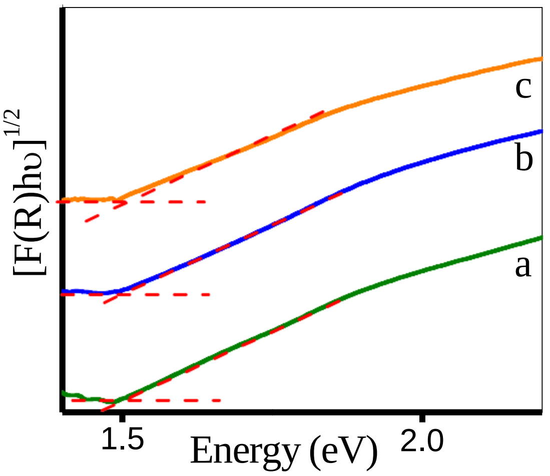

Fig. S29 Plots of $[F(R)h\nu]^{1/2}$ vs energy generated by Kubelka-Munk transformation of solid-state diffuse reflectance data of $SnSe_2$ nano-sheets obtained by thermolysis of $[Et_2Sn\{SeC_4H(Me\text{-}4,6)_2N_2\}_2]$ (**2**) in OLA at 210 °C for a) 2, b) 5 and c) 10 minutes, respectively for determining indirect band gap energies.

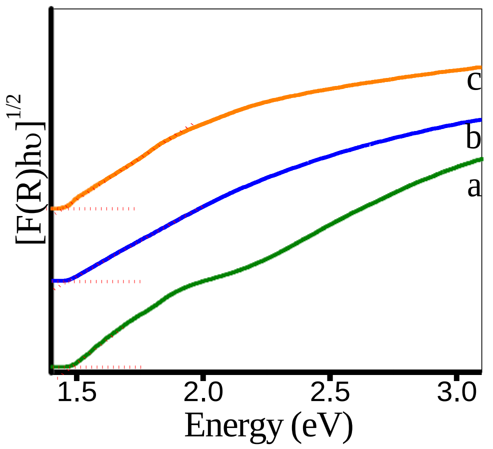

Fig. S30 Plots of $[F(R)h\nu]^{1/2}$ vs energy generated by Kubelka-Munk transformation of solid-state diffuse reflectance data of $SnSe_2$ nano-sheets obtained by thermolysis of $[{}^tBu_2Sn\{SeC_4H(Me\text{-}4,6)_2N_2\}_2]$ (**4**) in OLA at 210 °C for a) 2, b) 5 and c) 10 minutes, respectively for determining indirect band gap energies.

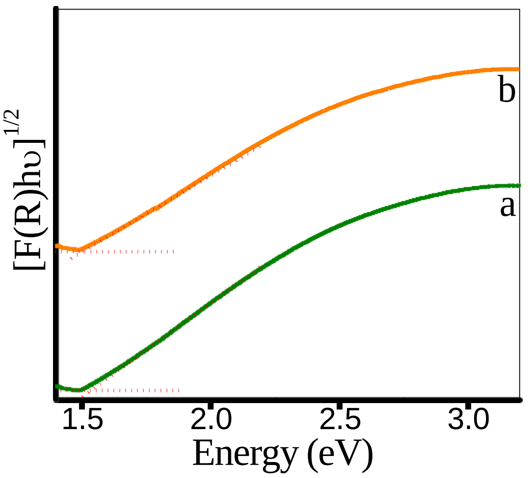

Fig. S31 Plots of $[F(R)h\nu]^{1/2}$ vs energy generated by Kubelka-Munk transformation of solid-state diffuse reflectance data of a) as-deposited $SnSe_2$ thin films obtained by AACVD of $[{}^tBu_2Sn\{SeC_4H(Me\text{-}4,6)_2N_2\}_2]$ (**4**) on silicon substrate at 375 °C for 1 h and b) annealed thin films to determine indirect band gap energies.

Table S1. Crystallographic and structural determination data for [$^{n}Bu_2Sn\{SeC_4H(Me\text{-}4,6)_2N_2\}_2$] (**3**).

	[$^{n}Bu_2Sn\{SeC_4H(Me\text{-}4,6)_2N_2\}_2$] (**3**)
Chemical formula	$C_{20}H_{32}N_4Se_2Sn$
Formula weight	605.11
Crystal size/mm^3	0.20 × 0.15× 0.05
Crystal system / space group	Triclinic /P1¯
Unit cell dimensions	
a/Å	11.659(6)
b/Å	16.166(17)
c/Å	29.13(3)
α	84.62(9)
β	84.17(5)
γ	70.44(7)
Volume/Å^3	5137(8)
Z	8
D_c/g cm^{-3}	1.565
μ/mm^{-1}	3.840
F(000)	2384
Limiting indices	$-8 \leq h \leq 15$
	$-19 \leq k \leq 21$
	$-37 \leq l \leq 37$
No. of reflections collected / unique	23556/ 4580
No. of data / restraints / parameters	23556/ 624/ 925
Final R_1, ωR_2 indices [$I > 2\sigma(I)$]	0.1132, 0.2392
R_1, ωR_2 (all data)	0.4531, 0.3834
Goodness of fit on F^2	0.906
CCDC No.	**1420614**

Table S2 Selected bond lengths (Å) and angles (°) for [$^{n}Bu_2Sn\{SeC_4H(Me\text{-}4,6)_2N_2\}_2$] (**3**).

Molecule a		Molecule b		Molecule c		Molecule d	
Sn1-Se1	2.609(4)	Sn2-Se3	2.581(4)	Sn3-Se5	2.599(4)	Sn4-Se7	2.575(4)
Sn1-Se2	2.601(4)	Sn2-Se4	2.583(4)	Sn3-Se6	2.595(4)	Sn4-Se8	2.582(4)
Sn1-N1	2.747(13)	Sn2-N5	2.844(16)	Sn3-N11	2.778(16)	Sn4-N15	2.979(16)
Sn1-N3	2.722(16)	Sn2-N7	3.042(18)	Sn3-N9	2.732(17)	Sn4-N13	2.885(16)
Sn1-C13	2.09(3)	Sn2-C33	2.25(3)	Sn3-C53	2.12(3)	Sn4-C73	2.05(2)
Sn1-C17	2.18(2)	Sn2-C37	2.15(2)	Sn3-C57	2.17(2)	Sn4-C77	2.12(2)
Se1-C7	1.769(14)	Se3-C21	1.801(13)	Se5-C41	1.815(14)	Se7-C61	1.812(15)
Se2-C1	1.806(11)	Se4-C27	1.800(14)	Se6-C47	1.832(14)	Se8-C67	1.812(13)
Se1-Sn1-Se2	91.43(15)	Se3-Sn2-Se4	89.68(12)	Se5-Sn3-Se6	92.49(16)	Se7-Sn4-Se8	90.26(12)
Se1-Sn1-N1	153.0(4)	Se4-Sn2-N5	150.8(4)	Se5-Sn3-N9	154.2(5)	Se8-Sn4-N13	59.9(4)
Se1-Sn1-N3	61.1(4)	Se4-Sn2-N7	58.6(4)	Se5-Sn3-N11	61.1(4)	Se8-Sn4-N15	149.6(3)
Se2-Sn1-N3	152.4(4)	Se3-Sn2-N7	148.3(4)	Se6-Sn3-N11	153.5(4)	Se7-Sn4-N15	59.6(3)
C13-Sn1-C17	126.9(11)	C37-Sn2-C33	126.0(10)	C57-Sn3-C53	125.5(11)	C73-Sn4-C77	125.6(11)
C13-Sn1-Se2	110.3(8)	C37-Sn2-Se3	111.5(6)	C57-Sn3-Se6	108.7(7)	C73-Sn4-Se7	107.5(9)
C17-Sn1-Se2	106.7(7)	C33-Sn2-Se3	109.2(9)	C53-Sn3-Se6	109.9(8)	C77-Sn4-Se7	111.3(8)
C13-Sn1-Se1	105.5(9)	C37-Sn2-Se4	109.3(7)	C57-Sn3-Se5	106.9(6)	C73-Sn4-Se8	108.1(8)
C17-Sn1-Se1	110.4(5)	C33-Sn2-Se4	104.8(10)	C53-Sn3-Se5	108.2(9)	C77-Sn4-Se8	108.3(7)
C7-Se1-Sn1	88.4(7)	C21-Se3-Sn2	89.8(6)	C41-Se5-Sn3	89.6(6)	C61-Se7-Sn4	92.9(6)
C1-Se2-Sn1	88.3(6)	C27-Se4-Sn2	94.3(7)	C47-Se6-Sn3	88.7(8)	C67-Se8-Sn4	91.6(7)
N1-Sn1-N3	145.9(6)	N5-Sn2-N7	150.5(5)	N9-Sn3-N11	144.7(6)	N13-Sn4-N15	150.5(5)
C13-Sn1-N1	84.6(9)	C37-Sn2-N5	84.6(8)	C57-Sn3-N9	84.9(7)	C73-Sn4-N13	80.9(10)
C17-Sn1-N1	80.8(6)	C33-Sn2-N5	85.3(11)	C53-Sn3-N9	81.1(10)	C77-Sn4-N13	84.0(8)
C13-Sn1-N3	81.3(8)	C37-Sn2-N7	81.6(7)	C57-Sn3-N11	80.8(7)	C73-Sn4-N15	86.8(9)
C17-Sn1-N3	83.2(7)	C33-Sn2-N7	81.9(10)	C53-Sn3-N11	80.8(7)	C77-Sn4-N15	81.6(8)

Table S3 XRD data for tin selenide nanosheets

S. No.	Complex	Duration of reaction in OLA	2θ	Corresponding plane	Lattice parameter	JCPDS File No.
1	[$Et_2Sn\{SeC_4H(Me-4,6)_2N_2\}_2$] (**2**)	2	14.36, 27.81, 30.72, 39.97, 44.15, 45.98, 47.76, 50.01, 52.52, 54.72, 57.79	(009), (104), (109), (1018), (0027), (0028), (111), (119), (1113), (0033), (209)	3.811, 55.22(8)	40-1465
2		5	14.35, 28.18, 29.70, 30.73, 40.05, 41.33, 44.00, 47.84, 52.00, 55.74, 57.87	(009), (105), (108), (109), (1018), (1019), (1021), (110), (1112), (202), (209)	3.811, 55.21(40)	40-1465
3		10	14.35, 27.07, 29.08, 30.70, 40.09, 44.12, 47.76, 50.08, 52.60, 57.86	(001), (100), (002), (101), (102), (003), (110), (111), (103), (201)	3.810, 6.141(7)	23-0602
4	[$^{n}Bu_2Sn\{SeC_4H(Me-4,6)_2N_2\}_2$] (**3**)	2	14.47, 27.05, 29.73, 30.73, 40.20, 41.30, 44.16, 45.29, 47.69, 49.94, 57.86	(009), (101), (108), (109), (1018), (1019), (0027), (1022), (110), (119), (209)	3.811, 54.99(31)	40-1465
5		5	14.47, 27.05, 29.7, 30.73, 40.05, 41.18, 43.70, 45.29, 47.69, 52.49, 55.89, 57.87	(009), (101), (108), (109), (1018), (1019), (1021), (1022), (110), (1113), (203), (209)	3.811, 55.15(32)	40-1465
6		10	14.35, 29.00, 30.70, 40.09, 44.12, 47.66, 52.60	(001), (002), (101), (102), (003), (110), (103)	3810, 6.147(6).	23-0602
7	[$^{t}Bu_2Sn\{SeC_4H(Me-4,6)_2N_2\}_2$] (**4**)	2	14.46, 30.80, 40.14, 47.77, 50.06, 52.61, 57.82	(009), (109), (1018), (111), (119), (1113), (209)	3.811, 55.24(17)	40-1465
8		5	14.36, 27.08, 30.72, 40.17, 44.35, 47.79, 50.16, 52.52, 57.78	(009), (101), (109), (1018), (0027), (110), (119), (1113), (209)	3.811, 55.19(16)	40-1465
9		10	14.35, 30.7, 40.09, 44.3, 47.7, 50.08, 52.60, 57.86	(001), (101), (102), (003), (110), (111), (103), (201)	3811, 6.146(6)	23-0602